DOI: 10.13009/EUCASS2019-167

Architectured materials for space applications: a computational tool for the parametric optimization of a three-dimensional lattice subjected to stiffness constraints

F. Ongaro[a], K. Mathis[b], F. Masson[b] and J. Dirrenberger[a]

[a]PIMM Lab, ENSAM/CNAM/CNRS UMR 8006, 151 Bd de l'Hôpital, 75013 Paris, France
[b]CNES-Launchers Directorate, 52 Rue Jacques Hillairet, 75612 Paris Cedex, France

federica.ongaro@ensam.eu · kevin.mathis@cnes.fr · frederic.masson@cnes.fr · justin.dirrenberger@ensam.eu

Abstract

Architectured materials, whose discrete configuration provides unique combinations of enhanced structural properties at low weight, solved a variety of technical challenges in material science, architecture, aerodynamics and mechanical engineering. This peculiar characteristic, together with a high degree of design freedom leading to the possibility to tailor their mechanical properties in each direction, makes them very promising in a vast number of industries including aerospace, automotive, marine and constructions. However, the use of architectured materials is conditional upon the development of appropriate constitutive models for revealing the complex relations between the parameters of the microstructure and the macroscopic behavior. Notwithstanding a great variety of analytical and numerical techniques have been proposed and discussed in recent years, explicit formulas for the effective mechanical properties are derived in a very small number of investigations. To provide a contribution in this limitedly explored research area, this paper describes the mathematical formulation and modelling technique leading to closed-form expressions for the effective stiffness of a three-dimensional lattice composed of identical hexatruss cells. The derived analytical relations, verified by performing experimental tests on a 3D-printed lattice, are then integrated into a parametric optimization problem for finding the optimal microstructure's parameters that meet a given set of stiffness requirements. This strategy offers a less computationally way to solve optimization problems for architectured materials and, as a practical example, the specific case of the Spacecraft-Launcher Damping Interface is considered. The developed theory, however, is general enough to be easily applied to different types of structures in the aerospace industry.

1. Introduction

1.1 Architectured materials: overview

Architectured materials, defined as a composition of two or more materials and space,[1] offer unique combinations of mechanical properties, like stiffness, strength or toughness, at low weight, providing the coexistence of what used to be antagonistic performances within a single homogeneous material.

Due to their peculiar configuration, arising from their discrete nature, architectured materials are very promising for engineering applications in a variety of industries including aerospace, automotive, marine and constructions. For example, the low density makes them ideal core materials in lightweight and high-performance sandwich panels used in aerospace components and sporting equipments, while the low compressive strength and high deformation capacity provide excellent shock mitigation and energy absorption characteristics in impulsive phenomena.

However, the use of architectured materials is conditional upon the development of appropriate constitutive models for revealing their effective properties. From this point of view, two sets of parameters affect their mechanical behavior: the first characterises the constituent material, the second is related to the geometric and topological properties of the microstruture. In addition, the formulation of a continuum model is hindered by the crucial passage from the microscopic discrete description to the coarse continuous one and, to overcome this problem, energy equivalence concepts and micro-macro relations in terms of forces and displacements are usually applied. Also, linear elasticity

DOI: 10.13009/EUCASS2019-167

and material isotropy, in conjunction with the underlying microstructure assumed to be governed by the classical beam theory,[2] are three commonly used simplifications that provide explicit stress-strain relations and help clarifying the basic mechanical aspects.

1.2 State of the art

Many authors studied the mechanical modelling of architectured materials and a great variety of techniques have been proposed and exhaustively discussed in recent years.[3–6] However, the most known and widely used micromechanical model is due to the pioneering contribution of Gibson & Ashby,[7,8] focusing on the deformation mechanism of a single cell subjected to different types of external loads. The authors, in particular, obtained first-order power-law relations between the microstructure's parameters and the macroscopic properties of a wide range of architectured materials by assuming infinitesimal strains and applying the standard beam theory to model the lattice' edges. An alternative approach to solve the crucial passage from micro to macro and to derive the constitutive model for two-dimensional microstructures subjected to in-plane deformations was adopted by Chen et al.[9] and Kumar & McDowell[10] where, as in Gibson & Ashby,[7,8] the discrete lattice is idealised as a sequence of Euler-Bernoulli beams while, in this case, the macroscopic description follows from an energy-based technique. In the framework of homogenization theory, Gonella & Ruzzene[11] interprets the discrete lattice according to the finite difference formalism and the equivalent continuum derives from the application of Taylor's series expansions of the nodal displacements and rotations, motivated by the multi-scale nature of the considered problem. Notions of crystals' theory[12] helped Hutchinson & Fleck,[13] Elsayed & Pasini,[14] Vigliotti & Pasini[15] to estimate the effective stiffness of different types of bi-dimensional lattice materials, represented as a pin-jointed infinite microtruss structure obtained by tessellating a unit cell into a periodic modular pattern. The suggested approach relies on the Cauchy-Born assumption[16] to express the lattice's nodal displacements in terms of the macroscopic strain field applied and to derive the homogenized properties.

Force- and energy equivalence-based techniques have also been applied to characterise the mechanical behavior of three-dimensional lattice materials. Zhu et al.,[17] for example, expressed the Young's modulus, shear modulus and Poisson's ratio of the tetrakeidecahedral lattice as a function of the relative density, while the mechanical performance of the octet-truss lattice is investigated in Deshpande et al.[18] and Challapalli & Ju[19] from a theoretical and numerical point of view. Both the effective elastic properties and collapse surfaces for buckling and plastic yielding are derived and verified by means of experimental observations. A more general analysis of three-dimensional periodic lattices is proposed in Vigliotti & Pasini[20] and Refai et al.,[21] where the authors employed a finite element-based homogenization method to determine the macroscopic elastic properties of open- and closed-cell lattices with different known topologies of the unit cell, as BCC, FCC and octet.

In the last decade, due to the advent of additive manufacturing technologies, several attempts have been made to further explore the potential advantages of architectured materials and special attention is given to the possibility to achieve optimised structures of actual use, in terms of tailored combinations of stiffness and strength. For instance, how to lower the value of the stiffness while increasing the strength, in order to obtain a lattice material that is easily deformed but resistant to rupture Haghpanah et al.[22] Also, as reported in Vigliotti & Pasini[23] with reference to the design of a cantilever bracket subjected to a point load, a proper selection of the microstructure's parameters allows the tunability of the macroscopic mechanical properties in different directions. Starting from the geometry and boundary conditions of the examined component, the authors set up a multiobjective optimization problem (MOO) to determine the optimal lattice material providing the maximisation of the bracket's stiffness while reducing its mass. Four lattice topologies have been considered, kagome, equilateral triangular and rectangular triangular, and, for each one, the optimized parameters have been obtained by reformulating the original MOO problem into a sequence of single objective optimization problems, solved with a discrete gradient-based method.[24] As suggested by the name, gradient-based optimization techniques use gradient informations to find the optimal solution and, despite being very popular in engineering, have several drawbacks including the difficulty to be efficiently implemented and the fact that only a local optimum can be identified.[24,25] A different way to solve optimization problems of lattice strutures, providing a better chance to find the global optimum, consists in adopting non-gradient optimization techniques, such as the evolutionary optimization algorithms.[24,26] These well established methods mimic the process of natural evolution by following the four basic steps of reproduction, mutation, recombination and selection[25] and, among them, the genetic algorithm[27] has found to be extremely robust, easy to implement and well suited for numerous structural engineering applications.[24,25] An abundance of literature exists in this field, as the work proposed by Vaissier et al.[28] focusing on the development of a genetic algorithm-based framework for the shape and topology optimization of a lattice structure used as a support in additive manufacturing. Referring the interested reader to Burczynski & Osyczka[29] for a more detailed discussion, two final examples include the application of the genetic algorithm to perform the parametric optimization of chiral lattices for flexible frames with various specifications and dimensions,[30] and the shape optimization of regular lattice structures, hexagonal, triangular and square, in order to obtain the maximum shear capacity.[31]

DOI: 10.13009/EUCASS2019-167

1.3 Scope and outline of the present paper

With reference to the applicability of architectured materials to design certain components of the Ariane Launcher, this work presents a computational tool for the parametric optimization of a three-dimensional lattice composed of identical hexatruss unit cells, subjected to a given set of stiffness requirements. The paper is organised in 6 sections, including this introduction. Initially, by modelling the examined lattice as a sequence of three-dimensional Euler-Bernoulli beams, an energy-based approach coupled with the Cauchy-Born assumption provide, in Section 2, closed-form expressions for the macroscopic stiffness. Such relations, verified by comparison with the outcome of the experimental campaign described in Section 3, are then integrated in the parametric optimization problem described in Section 4. Here, in particular, the optimal parameters of the microstructure are derived by optimizing a system of three analytical equations, i.e., the effective stiffness in the three directions, and this strategy, based on the genetic algorithm, offers a less computationally expensive way to solve optimization problems for architectured materials since a change in the parameters does not require a re-generation of the lattice. Finally, Section 5 summarises the main findings.

2. The hexatruss lattice: theoretical modelling and homogenization of the discrete system

2.1 Overview

This paper focuses on the three-dimensional auxetic microstructure presented by Dirrenberger et al.,[32] generated by tessellating a hexatruss unit cell (Fig. 1) through the space along three independent periodic vectors $\mathbf{l}_1$, $\mathbf{l}_2$, $\mathbf{l}_3$. In the global reference system, defined by the unit orthonormal vectors $\boldsymbol{e}_1$, $\boldsymbol{e}_2$, $\boldsymbol{e}_3$ and by the coordinate system (X, Y, Z), the components of the lattice vectors are

$$\mathbf{l}_1 = \begin{bmatrix} L_1 & 0 & 0 \end{bmatrix}^T, \quad \mathbf{l}_2 = \begin{bmatrix} 0 & L_2 & 0 \end{bmatrix}^T, \quad \mathbf{l}_3 = \begin{bmatrix} 0 & 0 & L_3 \end{bmatrix}^T, \tag{1}$$

with L_1, L_2, L_3 the overall dimensions of the cell (the lattice size).

The resulting system can be conceived as a collection of discrete elements connected at nodes locations periodically arranged. In particular, two classes of nodes can be identified: the internal nodes and the boundary nodes. The first connect elements of only a single cell while the second connect elements of confining cells. Also, due to the periodicity of the lattice configuration, the boundary nodes are corresponding along the lattice vectors and, as outlined in the following sections, such nodes will be subjected to the imposition of kinematic constraints in order to preserve the periodicity of the deformed lattice.

Finally, from a mechanical point of view, the examined microstructure is treated as an interconnected network of three-dimensional Euler-Bernoulli beams having circular cross-section of radius r and made of a linear elastic isotropic material with Young's modulus E_s, Poisson's ration ν_s and shear modulus G_s, as explained in the next section.

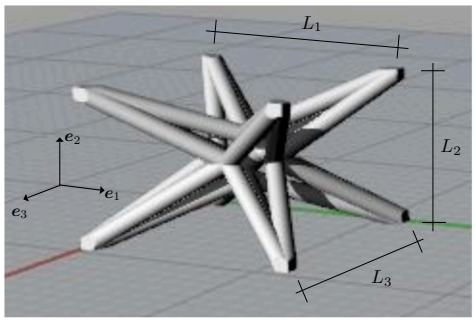

Figure 1: The hexatruss unit cell

DOI: 10.13009/EUCASS2019-167

2.2 The three-dimensional Euler-Bernoulli beam element

Let us focus on the e-th Euler-Bernoulli beam element illustrated in Figure 2.

In the global reference ($\boldsymbol{e}_1$, $\boldsymbol{e}_2$, $\boldsymbol{e}_3$), the configuration of the considered element is known by specifying the coordinates of its end nodes, I and J. However, to analyse the generic component it is more convenient using a local reference system, specific to the considered beam and closely dependent to its geometry. Such reference is defined by three orthonormal unit vectors $\boldsymbol{\eta}_1^e$, $\boldsymbol{\eta}_2^e$, $\boldsymbol{\eta}_3^e$ (Fig. 2), and by the coordinate reference system (x, y, z).

It should be noted that, hereinafter, the local notation will be adopted and the extreme nodes of the beam will be denoted by the indices i and j. Similarly, lowercase letters will be used to differentiate the local variables from the global ones.

Regarding the kinematics of the three-dimensional Euler-Bernoulli beam, each node has six degrees of freedom: three translations, u^e, v^e and w^e, and three rotations, φ_x, φ_y and φ_z. Thus, the following 12x1 vector completely describes the element nodal displacements:

$$\mathbf{d}^e := \begin{bmatrix} \mathbf{d}_i^e \\ \mathbf{d}_j^e \end{bmatrix} = \begin{bmatrix} u_i^e & v_i^e & w_i^e & \varphi_{xi}^e & \varphi_{yi}^e & \varphi_{zi}^e & u_j^e & v_j^e & w_j^e & \varphi_{xj}^e & \varphi_{yj}^e & \varphi_{zj}^e \end{bmatrix}^T. \tag{2}$$

In terms of energetics, the elastic strain energy of the Euler-Bernoulli beam element takes the form

$$w^e := \frac{1}{2}(\mathbf{d}^e)^T \cdot \mathbf{k}^e \mathbf{d}^e, \tag{3}$$

with $\mathbf{k}^e$ the element stiffness matrix expressed in the local reference system.[33]

Finally, similarly to Equation (2), the forces and couples acting at the extreme nodes of the beam (Fig. 2b),

$$\mathbf{f}^e := \begin{bmatrix} \mathbf{f}_i^e \\ \mathbf{f}_j^e \end{bmatrix} = \begin{bmatrix} f_{xi}^e & f_{yi}^e & f_{zi}^e & m_{xi}^e & m_{yi}^e & m_{zi}^e & f_{xj}^e & f_{yj}^e & f_{zj}^e & m_{xj}^e & m_{yj}^e & m_{zj}^e \end{bmatrix}^T, \tag{4}$$

are derived from the classical relation

$$\mathbf{f}^e := \mathbf{k}^e \, \mathbf{d}^e. \tag{5}$$

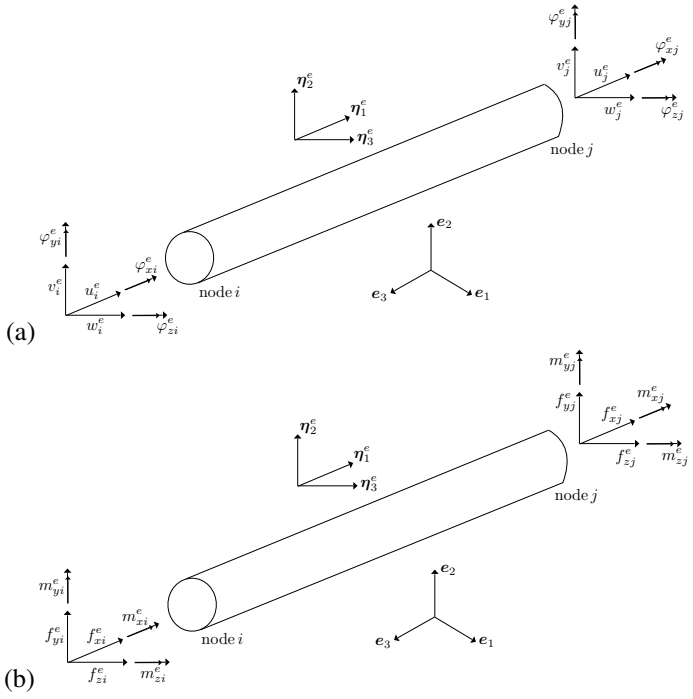

Figure 2: The Euler-Bernoulli beam element in the local reference system: (a) degrees of freedom, (b) forces and couples

DOI: 10.13009/EUCASS2019-167

2.3 The hexatruss unit cell: description and energetics

The typical approach to the continuum modelling of architectured materials includes the selection of a *Representative Volume Element* (RVE) that, in investigating materials with a periodic microstructure as in the present paper, coincides with the repetitive unit cell of the tessellation.[34]

In the examined case, in particular, the unit cell is composed by the eight boundary nodes 1, 2, 3, 4, 5, 6, 7, 8 linked to the internal ones 9, 10, 11, 12, 13, 14 by the line elements (Fig. 3)

$$1-9, \quad 2-9, \quad 6-9, \quad 5-9 \qquad \text{(Face Front)}$$

$$4-10, \quad 3-10, \quad 7-10, \quad 8-10 \qquad \text{(Face Back)}$$

$$1-11, \quad 2-11, \quad 3-11, \quad 4-11 \qquad \text{(Face Bottom)}$$

$$5-12, \quad 6-12, \quad 7-12, \quad 8-12 \qquad \text{(Face Top)}$$

$$1-13, \quad 4-13, \quad 8-13, \quad 5-13 \qquad \text{(Face Left)}$$

$$2-14, \quad 3-14, \quad 7-14, \quad 6-14 \qquad \text{(Face Right)}$$

that, in the global reference system $(\boldsymbol{e}_1, \boldsymbol{e}_2, \boldsymbol{e}_3)$, are described by the vectors

$$\mathbf{b}_{A-B} = \mathbf{p}_B - \mathbf{p}_A, \tag{6}$$

being $\mathbf{p}_A$ and $\mathbf{p}_B$, respectively, the position vectors of the extreme nodes of the element, A and B the index listed in Table (1). For sake of clarity, it is worth noting that, in Equation (6), $\mathbf{p}_A$ and $\mathbf{p}_B$ are expressed in the global reference system so that, to differentiate the global variables from the local ones (cf. Section 2.2), uppercase letters, i.e., indices A and B, are used.

As anticipated in Section 2.1, the connecting elements are represented as three-dimensional Euler-Bernoulli beams and this assumption, along with an energy-based approach, provide, in the following section, closed-form expressions for the effective elastic moduli of the examined lattice.

Finally, in terms of energetics, for any given deformation the elastic energy representative of the whole discrete structure, W, can be evaluated from that of the beams composing the unit cell of the periodic array. Specifically, after writing Equation (3) in the global reference system and summing the energetic contribution of each beam, it emerges

$$W = \frac{1}{2}\mathbf{D}^T \cdot \mathbf{K}\mathbf{D}, \tag{7}$$

with

$$\mathbf{D} := \begin{bmatrix} \mathbf{D}_1 \\ \mathbf{D}_2 \\ \cdots \\ \mathbf{D}_{14} \end{bmatrix} = \begin{bmatrix} U_1 & V_1 & W_1 & \Phi_{X1} & \Phi_{Y1} & \Phi_{Z1} & \cdots & \Phi_{Z14} \end{bmatrix}^T \tag{8}$$

the global displacements vector, collecting the displacements and rotations of all nodes of the unit cell and $\mathbf{K}$ the global stiffness matrix, assembled by adopting standard techniques of the finite element method.[33]

Table 1: The indices A and B identifying the unit cell elements

B	A
9	1, 2, 6, 5
10	4, 3, 7, 8
11	1, 2, 3, 4
12	5, 6, 7, 8
13	1, 4, 8, 5
14	2, 3, 7, 6

DOI: 10.13009/EUCASS2019-167

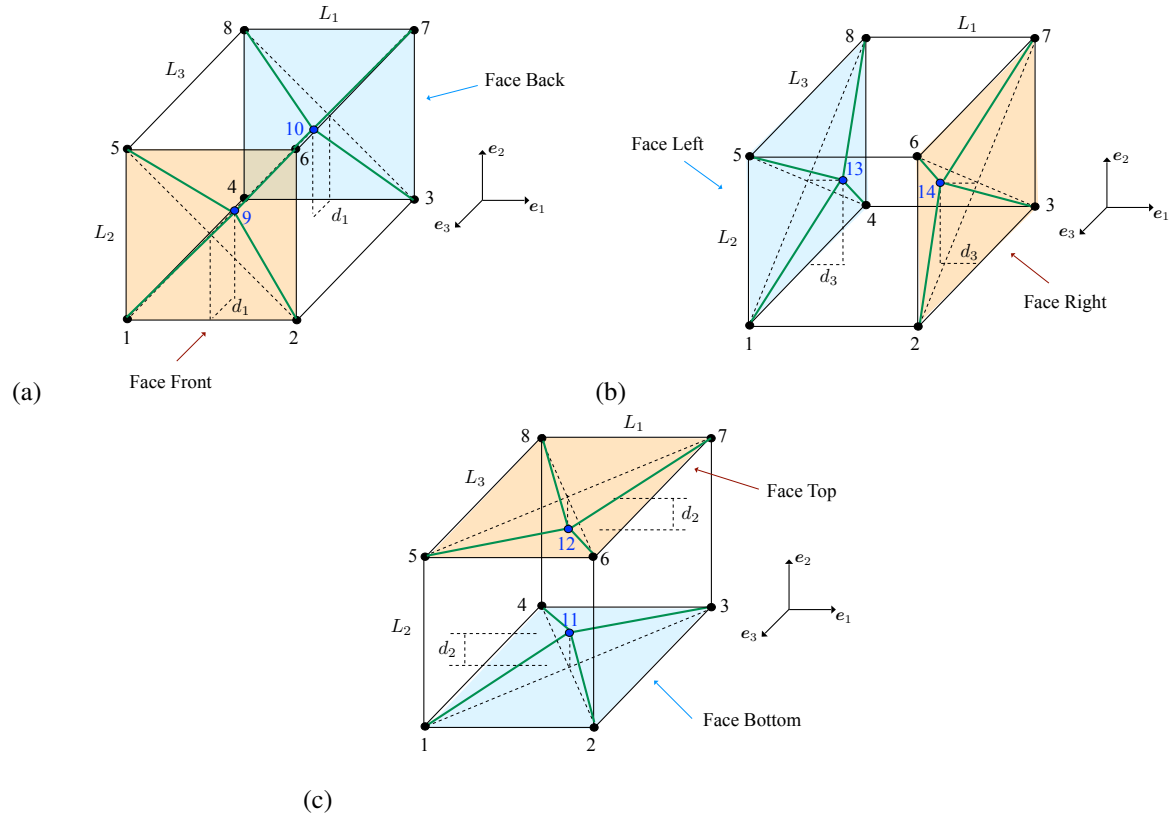

Figure 3: The beams composing the hexatruss unit cell: (a) Face Front and Face Back, (b) Face Right and Face Left, (c) Face Top and Face Bottom

2.4 Continuum modelling: effective stiffness

The continuum form of W can be derived by adopting the Cauchy-Born relation,[20,23] providing a viable approach to express the displacements of each node of the unit cell as a function of the macroscopic strain field applied,

$$\mathbf{E} := \begin{bmatrix} \varepsilon_{11} & \varepsilon_{12} & \varepsilon_{13} \\ \varepsilon_{12} & \varepsilon_{22} & \varepsilon_{23} \\ \varepsilon_{13} & \varepsilon_{23} & \varepsilon_{33} \end{bmatrix}. \tag{9}$$

Specifically, if we introduce the vector $\mathbf{D}_R$ collecting the displacements of the generic R-th node within the cell and the corresponding position vector $\mathbf{p}_R$, the Cauchy-Born relation, in its general form, can be expressed as

$$\mathbf{D}_R = \mathbf{D}_0 + \mathbf{E} \cdot (\mathbf{p}_R - \mathbf{p}_0), \tag{10}$$

with $\mathbf{D}_0$ and $\mathbf{p}_0$, in turn, the displacements vector and position vector of an appropriately selected unit cell's independent node. Also, by enforcing the equilibrium conditions on the nodal forces,[20] it is possible to calculate the displacements $\mathbf{D}_0$ in terms of $\mathbf{E}$.

Notwithstanding alternative choices of the independent node are possible, in the proposed study the boundary node 4 has been selected as independent node, leading to

$$\mathbf{D}_R = \mathbf{D}_4 + \mathbf{E} \cdot (\mathbf{p}_R - \mathbf{p}_4), \qquad R = 1, 2, ..., 14. \tag{11}$$

This assumption, in conjunction with Equation (11), provide an easy way to impose kinematic conditions on the boundary nodes of the cell that, as anticipated in Section 2.1, coincide with the application of periodic boundary conditions in order to enforce the periodicity of the deformed configuration.

Substituting Equation (11) into (7) and dividing the expression that turns out from the calculation by the volume of the unit cell, $V = L_1 L_2 L_3$, give the strain energy density in the continuum approximation, w. It emerges that w is a quadratic form of the infinitesimal strains ε_{ij},

$$w = w\left(\varepsilon_{ij}\right), \quad i, j = 1, 2, 3, \tag{12}$$

DOI: 10.13009/EUCASS2019-167

and, as in classical continuum mechanics, enables to derive the components of the macroscopic stiffness tensor of the lattice,

$$E_{ijhk} = \frac{\partial^2 w}{\partial \varepsilon_{ij}\, \partial \varepsilon_{hk}}, \quad i, j, h, k = 1, 2, 3. \tag{13}$$

and the corresponding effective elastic constants. In terms of effective Young's moduli, main focus of the present paper, Equation (13) gives

$$E_1 \equiv E_{1111} = \frac{\partial^2 w}{\partial \varepsilon_{11}\, \partial \varepsilon_{11}}, \quad E_2 \equiv E_{2222} = \frac{\partial^2 w}{\partial \varepsilon_{22}\, \partial \varepsilon_{22}}, \quad E_3 \equiv E_{3333} = \frac{\partial^2 w}{\partial \varepsilon_{33}\, \partial \varepsilon_{33}}, \tag{14}$$

with E_1, E_2, E_3, on order, the effective Young's moduli in the directions $\boldsymbol{e}_1$, $\boldsymbol{e}_2$ and $\boldsymbol{e}_3$.

As expected, the effective constants are strongly affected by the geometrical and mechanical properties of the microstructure and, from this point of view, the advantage of the proposed theory is that an explicit relation between the microstructure's parameters and the macroscopic properties can be obtained. Specifically, it emerges

$$\begin{aligned} E_1 &= E_1\,(L_1,\, L_2,\, L_3,\, r,\, d_1,\, d_2,\, d_3)\,, \\ E_2 &= E_2\,(L_1,\, L_2,\, L_3,\, r,\, d_1,\, d_2,\, d_3)\,, \\ E_3 &= E_3\,(L_1,\, L_2,\, L_3,\, r,\, d_1,\, d_2,\, d_3)\,, \end{aligned} \tag{15}$$

with r denoting the radius of the beam's cross-section, L_i and d_i, $i = 1, 2, 3$, the parameters defined in Figure (3).
To maintain the paper focused and not unnecessarily long, the complete expressions of E_1, E_2, E_3 is reported in Appendix A.

3. Model validation: the experimental campaign

As seen in the previous section, the effective properties of the hexatruss lattice can be predicted by knowing the constitutive laws and spacial distribution of its components.

Before addressing the optimization problem in order to find the optimal microstructure's parameters satisfying a given set of stiffness constraints (cf. Section 4), the proposed analytical results in Equation (15) are verified by comparison with those obtained by performing the experimental tests described in the following.

3.1 Description of the samples

As illustrated in Figure (4), the experimental tests have been conducted on a 3D-printed 3×3×3 unit cell hexatruss lattice and, to obtain an estimation of the effective stiffness in the directions $\boldsymbol{e}_1$, $\boldsymbol{e}_2$ and $\boldsymbol{e}_3$, coinciding with the three principal directions of the unit cell, the configurations listed below have been investigated (Fig. (5)):

- Configuration C1: to consider the direction $\boldsymbol{e}_1$ and derive E_1,
- Configuration C2: to consider the direction $\boldsymbol{e}_2$ and derive E_2,
- Configuration C3: to consider the direction $\boldsymbol{e}_3$ and derive E_3.

Aiming at obtaining a good quality of the printed samples, a unit cell with overall dimensions ($L_1 \times L_2 \times L_3$) of 9.6 mm × 11.52 mm × 7.68 mm has been selected, leading to

- Configuration C1 (length × width × height): 34.56 mm × 23.04 mm × 28.8 mm,
- Configuration C2 (length × width × height): 28.8 mm × 23.04 mm × 34.56 mm.
- Configuration C3 (length × width × height): 28.8 mm × 34.56 mm × 23.04 mm,

while, in terms of radius r and position of the internal nodes, d_1, d_2, d_3, the following values have been adopted: $r = 0.45$ mm, $d_1 = 2.8$ mm, $d_2 = 2.2$ mm, $d_3 = 3.3$ mm.

In addition, to account for possible errors associated with the 3D-printing process, three copies of each configuration have been printed and tested.

Finally, regarding the constituent material, two different polymers have been used to print the samples: PLA (Polylactic Acid) and PET (Polyethylene Terephthalate) having, on order, Young's modulus of

$$E_{PLA} = 1.3\,\text{GPa}, \qquad E_{PET} = 0.8\,\text{GPa}, \tag{16}$$

values obtained by conducting traction tests according to the ASTM standards.[35]

DOI: 10.13009/EUCASS2019-167

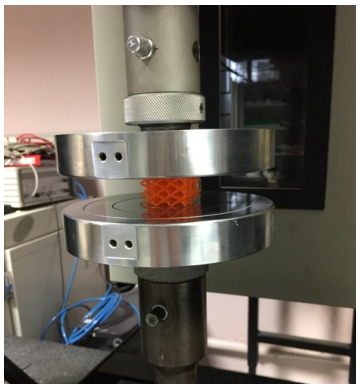

Figure 4: Polymeric samples: compression tests

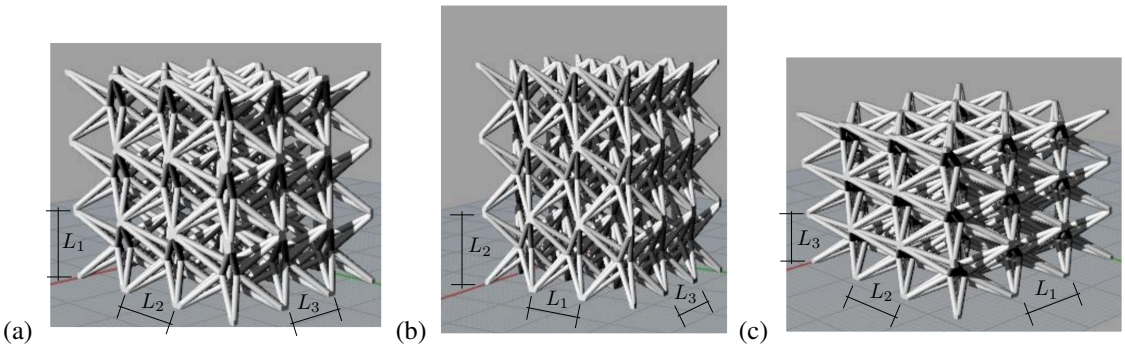

Figure 5: The three different configurations of the samples involved in the mechanical tests: (a) configuration C1, (b) configuration C2, (c) configuration C3

3.2 Methodology

3.2.1 Type of tests

In order to mechanically characterise the 3D-printed samples, compression tests have been considered and, to validate the theoretical approach in Section 2, force-displacement and stress-strain curves have been analysed. Specifically, the following type of test have been performed:

- uniaxial compression tests at room temperature,
- displacement-controlled tests at a displacement rate of 0.5 mm/min,
- only elastic deformations involved, $\varepsilon_{max} = 1\,\%$,
- no interfaces between the sample and the test bench

and the testing machine *Instron 5881* has been employed.

3.2.2 Objectives

The aim of the tests was to evaluate the effective stiffness of the hexatruss lattice in the three principal directions $\boldsymbol{e}_1$, $\boldsymbol{e}_2$, $\boldsymbol{e}_3$, measured in terms of effective Young's moduli denoted, respectively, by E_1, E_2 and E_3. The latter, in particular, have been derived by:

i) recording, during the test, both the displacement, ΔL, and resulting load, F, applied to the sample;

ii) generating, with the sample geometry, a stress-strain curve, being the engineering strain, ε, and the engineering stress, σ, given by

$$\varepsilon := \frac{\Delta L}{L_0} \quad \text{and} \quad \sigma := \frac{F}{A_0}, \tag{17}$$

with L_0 and A_0, in turn, the initial height of the sample and its initial cross-sectional area normal to the loading direction;

DOI: 10.13009/EUCASS2019-167

iii) finally, focusing on the slope of the linear portion of the stress-strain curve that coincides, in the elastic regime, with the Young's modulus E of the considered material. Namely,

$$E = \frac{\sigma}{\varepsilon}. \tag{18}$$

3.3 Results and discussion

The outcome of the experimental campaign is presented in Tables 2 and 3, where the comparison between the experimental results and the theoretical predictions in Equation (15) is also provided.

For sake of clarity, it should be noted that the analytical values reported in Tables 2 and 3 are obtained by substituting in Equation (15) the quantities

$$\begin{gathered} r = 0.45\,\text{mm}, \\ L_1 = 9.6\,\text{mm}, L_2 = 11.52\,\text{mm}, L_3 = 7.68\,\text{mm}, \\ d_1 = 2.8\,\text{mm}, d_2 = 2.2\,\text{mm}, d_3 = 3.3\,\text{mm} \end{gathered} \tag{19}$$

and

$$\begin{aligned} E_s \equiv E_{PLA} &= 1.3\,\text{GPa, (Table 2)}, \\ E_s \equiv E_{PET} &= 0.8\,\text{GPa, (Table 3)}, \end{aligned} \tag{20}$$

coinciding with the geometrical, the first, and mechanical, the second, parameters defining the unit cell adopted in the experimental tests.

As it can be seen, it generally emerges a good agreement between the theoretical and experimental results and, as expected, the theoretical values overestimate the experimental ones. From this point of view, the difference is mainly related to the quality of the 3D-printed samples that, differently from the analytical model where the beams are assumed to be perfectly homogeneous and without defects, in some cases present some imperfections, i.e., small parts missing, not perfectly homogeneous or beams not perfectly connected at the nodes.

However, taking into account the very close comparison in Tables 2 and 3, it can be said that the experimental tests validate the theoretical expressions in Equation (15) and can thus be employed to formulate the optimization problem in the next section.

Table 2: PLA samples, Young's moduli. Comparison between the theoretical and experimental results

	Experiments	Theoretical results
E_1 (MPa)	2.72	3.09
E_2 (MPa)	4.55	4.79
E_3 (MPa)	1.32	1.34

Table 3: PET samples, Young's moduli. Comparison between the theoretical and experimental results

	Experiments	Theoretical results
E_1 (MPa)	1.81	1.90
E_2 (MPa)	2.71	2.95
E_3 (MPa)	0.90	0.92

DOI: 10.13009/EUCASS2019-167

4. Parametric optimization

4.1 Problem description

As anticipated in Section 1, in this paper the parametric optimization of the hexatruss lattice is performed with reference to the design of the Ariane Launcher and, in particular, the specific case of the Spacecraft-Launcher Damping Interface (LALS) is considered. An extended set of requirements is expected for the LALS, in terms of geometry, maximal density, stiffness, mechanical damping and load withstanding. Leaving the other aspects for future research investigations, here, for simplicity, only the maximal density,

$$\rho_{req} \leq \rho_{max} = 1.9\,\mathrm{g/cm^3} \tag{21}$$

and stiffness,

$$\begin{aligned} E_1^{req} &= 8\,\mathrm{MPa} \pm 0.8\,\mathrm{MPa}, \\ E_2^{req} &= 15\,\mathrm{MPa} \pm 3\,\mathrm{MPa}, \\ E_3^{req} &= 0.4\,\mathrm{MPa} \pm 0.08\,\mathrm{MPa} \end{aligned} \tag{22}$$

requirements are considered, being ρ_{req} and E_1^{req}, E_2^{req}, E_3^{req}, respectively, the required values of the density and of the effective Young's moduli in the directions $\boldsymbol{e}_1$, $\boldsymbol{e}_2$, $\boldsymbol{e}_3$.

Our aim consists in finding the optimal parameters of the microstructure that meet the specifications listed in Equations (21), (22) and, to do so, the following multiobjective optimization problem has been formulated:

$$\text{Find } \mathcal{P} = \{L_1,\, L_2,\, L_3,\, r,\, d_1,\, d_2,\, d_3\}$$

$$\text{To minimize } f(\mathcal{P}) := \begin{cases} E_1(\mathcal{P}) - E_1^{req} \\ E_2(\mathcal{P}) - E_2^{req} \\ E_3(\mathcal{P}) - E_3^{req} \end{cases}$$

$$\text{Subjected to } \begin{cases} \mathcal{G}_1 \equiv \quad r \in [r_{min},\, r_{max}] \\ \mathcal{G}_2 \equiv \quad L_1,\, L_2,\, L_3 \in [L_{min},\, L_{max}] \\ \mathcal{G}_3 \equiv \begin{cases} d_1 \in \left[d_1^{min},\, d_1^{max}\right] \\ d_2 \in \left[d_2^{min},\, d_2^{max}\right] \\ d_3 \in \left[d_3^{min},\, d_3^{max}\right] \end{cases} \end{cases}$$

with $\mathcal{P}$ the design variables, defined in Section 2, that have to be optimized, $f(\mathcal{P})$ the objective function, expressed in terms of the analytical relations derived in Equation (15), $\mathcal{G}_1$, $\mathcal{G}_2$ and $\mathcal{G}_3$ the constraints introduced to limit the parameters' value to a range of realistic significance. Specifically, $\mathcal{G}_1$ and $\mathcal{G}_2$ are related to manufacturing limits, r_{min} and L_{min}, and to the multiscale approach of the present paper, where the length of scale of the microstructure is assumed to be much smaller than the length of scale of the component, r_{max} and L_{max}. Finally, $\mathcal{G}_3$ assures the suitability of the microstructure, where all the hexatruss cells must have all the nodes in the correct position.

In formulating the optimization problem, the maximal density requirement has been neglected, being easily satisfied just by employing architectured materials (cf. Section 4.3).

4.2 Solution method

The parametric optimization problem previously described has been solved by using the genetic algorithm and, in particular, the in-built MATLAB function *gamultiobj* has been employed. Such function is based on the genetic algorithm and allows the user to efficiently solve a multiobjective optimization problem with several optimization variables, as in the present case.

Being a detailed description of the working principle of the genetic algorithm well beyond the scope of the present paper, in Figure 6 only a schematic representation of the method is reported. As illustrated in Figure 6, the genetic algorithm starts by creating an initial random population of potential solutions, $P(t)$, whose individuals are then

DOI: 10.13009/EUCASS2019-167

ranked according to their fitness, i.e., their value of the objective function that, for a minimization problem, has to be as smaller as possible. If the termination condition is not satisfied, for example, if the maximum number of iterations is not reached, the three operators of reproduction, crossover and mutation are applied to $P(t)$ in order to create a new generation of individuals, $P(t+1)$. The reproduction operator, in particular, selects the 'most fit' individuals of $P(t)$ to form a matching pool so that, similarly to the principles of natural evolution, the individuals with the best traits have a higher probability to survive. The second operator, crossover, generates the individuals of $P(t+1)$ by randomly mixing the best traits of the individuals in the matching pool while, for maintaining diversity in the population, the mutation operator alters the traits of some individuals in $P(t+1)$ in order to create, hopefully, a better individual. Similarly to $P(t)$, the generation $P(t+1)$ is then ranked and the process described above is repeated until the termination condition is met and the algorithm converges to the optimal solution of the problem.

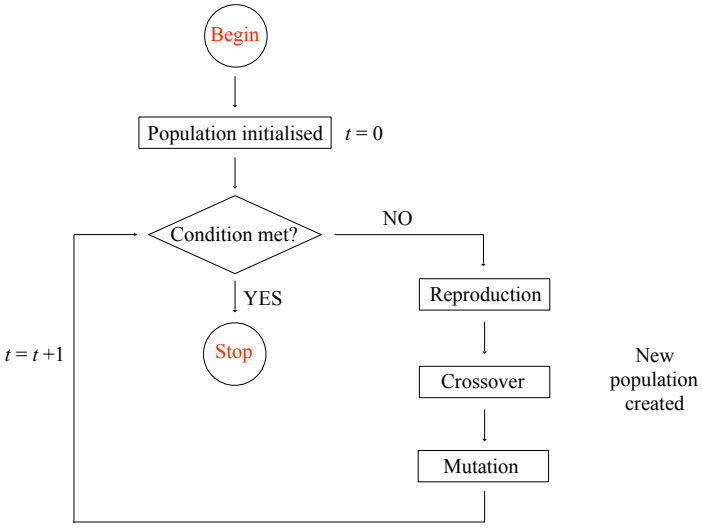

Figure 6: The genetic algorithm: working principle

4.3 Results and discussion

The results of our investigations are reported in Table 5, where titanium Ti64 with[36] Young's modulus $E_s = 97$ GPa, Poisson's ratio $\nu_s = 0.3$ and density $\rho_s = 4.5$ g/cm^3 has been assumed as constituent material of the microstructure. 6 different cases have been considered by changing the size of the population or the bounds of the parameters' value, as summarised in Table 4 where, for conciseness, the limits ℓ_1 and ℓ_2 are given by:

$$\ell_1 := \begin{cases} 3\,\text{mm} \le L_1, L_2, L_3 \le 20\,\text{mm} \\ 0.13\,\text{mm} \le r \le 0.5\,\text{mm} \\ 0 < d_1 < L_3/2 \\ 0 < d_2 < L_2/2 \\ 0 < d_3 < L_1/2 \end{cases} \qquad \ell_2 := \begin{cases} 3\,\text{mm} \le L_1, L_2, L_3 \le 15\,\text{mm} \\ 0.13\,\text{mm} \le r \le 0.5\,\text{mm} \\ 0 < d_1 < L_3/2 \\ 0 < d_2 < L_2/2 \\ 0 < d_3 < L_1/2 \end{cases} \tag{23}$$

As a general observation, it can be said that Table 5 suggests the possibility, for the hexatruss lattice, to satisfy the three stiffness requirements expected for the LALS. This is a great advantage of the examined microstructure since the values of the required stiffness in the three directions are very different from each other, making their simultaneous satisfaction very challenging. Slightly different solutions emerge in the investigated cases. However, comparing the values of L_1, L_2, L_3 and of d_1, d_2, d_3, reveals that, in each example, the following relations hold:

$$L_2 \approx 1.42\,L_1, \qquad L_3 \approx 0.46\,L_1, \tag{24}$$

$$d_2 \approx 0.45\,d_1, \qquad d_3 \approx 1.4\,d_1. \tag{25}$$

In a practical context, this finding, in conjunction with Equation (15), could assist the designer in the selection of the microstructure's parameters in order to reach a prescribed value of macroscopic stiffness. Finally, as anticipated in Section 4.1, all the configurations listed in Table 5 have a density of $\rho \approx 0.1$ g/cm^3, value that is well beyond the required limit in Equation (21).

DOI: 10.13009/EUCASS2019-167

Table 4: Parametric optimization of the hexatruss: considered cases

Case	Limits	Population's size
1	ℓ_1	2000
2	ℓ_1	4000
3	ℓ_1	6000
4	ℓ_1	8000
5	ℓ_2	8000
6	ℓ_2	4000

Table 5: Parametric optimization of the hexatruss lattice: results

	case 1	case 2	case 3	case 4	case 5	case 6
L_1 (mm)	12.16	12.22	12.04	12.13	10.2	10.1
L_2 (mm)	17.17	17.43	17.03	17.36	14	14.1
L_3 (mm)	5.63	5.68	5.58	5.64	4.7	4.7
r (mm)	0.19	0.19	0.19	0.19	0.15	0.15
d_1 (mm)	2.54	2.80	2.6	2.74	1.42	1.9
d_2 (mm)	1.18	1.32	1.2	1.2	0.66	0.89
d_3 (mm)	3.6	4.0	3.66	3.73	1.96	2.68
E_1 (MPa)	8	8	8	8	8	8
E_2 (MPa)	15	15	15	15	15	15
E_3 (MPa)	0.4	0.4	0.4	0.4	0.4	0.4
ρ (g/cm^3)	0.1	0.1	0.1	0.1	0.09	0.09

5. Conclusions

Because of their discrete configuration, architectured materials offer unique combinations of improved mechanical properties, like stiffness, strength or toughness, at low weight. This unusual characteristic, in conjunction with the possibility to tailor their mechanical properties in each direction, makes them very promising in a vast number of engineering fields including aerospace, automotive, marine and constructions. Differently from the traditional homogeneous materials, architectured materials require appropriate constitutive models for revealing the complex relations between the microstructure's parameters and the macroscopic properties. A great deal of effort has gone in this direction and, in the literature, a variety of techniques have been recently proposed and discussed. Different methods and assumptions have been suggested, however, only in a very limited number of investigations, closed-form expressions for the effective mechanical properties are provided. Such relations, if available, would facilitate the designer in the selection of the material that best suits a given requirement.

To help filling this research gap, this paper deals with the analysis of a three-dimensional lattice made of identical hexatruss cells. In the framework of linear elasticity and by modelling the microstructure as a sequence of three-dimensional Euler-Bernoulli beams, an energetic approach leads to explicit expressions for the effective elastic properties. To obtain a more mathematically tractable problem, the Cauchy-Born assumption is used to represent the nodal degrees of freedom as a function of the applied macroscopic strain components. This allows to write the elastic energy of the discrete system as a quadratic function of them and, as in classical mechanics, enables to derive the macroscopic stiffness tensor of the lattice and the corresponding elastic moduli. The predicted results are then verified by comparison with the outcome of the experimental tests performed and it emerges a very good agreement.

With reference to the specific case of the Spacecraft-Launcher Damping Interface (LALS), a parametric optimization of the hexatruss lattice is also reported. The aim is to obtain the optimal parameters of the microstructure satisfying a given set of stiffness requirements expected for the LALS. To do so, a multiobjective optimization problem has been formulated by including the analytical equations previously derived and the genetic algorithm has been selected to solve the problem. This approach, easily applied to different types of structures in the aerospace industry, offers an efficient and less computationally expensive way to derive the optimal parameters since the re-generation and corresponding analysis of the lattice is not required at each iteration.

DOI: 10.13009/EUCASS2019-167

Appendix A

$$
\begin{aligned}
E_1 &= \frac{16A\left(\sqrt{p_1}+\sqrt{p_2}+\sqrt{p_3}\right)}{L_2^2L_3^2p_1^{5/2}p_2^{5/2}p_3^{5/2}}\left(\left(EAL_1^2p_5+48EI\left(p_6+4d_2^2p_1^{5/2}\right)\right)p_3^{5/2}+64d_3^6EAp_1^{5/2}p_2^{5/2}+16d_3^4EAp_4+192d_3^2EIp_4\right),\\
E_2 &= \frac{16A\left(\sqrt{p_1}+\sqrt{p_2}+\sqrt{p_3}\right)}{L_2^2L_3^2p_1^{5/2}p_2^{5/2}p_3^{5/2}}\left(4d_3^2\left(48EI+EAL_2^2\right)p_1^{5/2}p_2^{5/2}+48EIp_7+EA\left(p_8+p_9\right)\right),\\
E_3 &= \frac{16A\left(\sqrt{p_1}+\sqrt{p_2}+\sqrt{p_3}\right)}{L_2^2L_3^2p_1^{5/2}p_2^{5/2}p_3^{5/2}}\left(192d_3^2EIp_1^{5/2}p_2^{5/2}+EAp_1p_2p_3p_{10}+48EIp_{11}\right),
\end{aligned}
\tag{26}
$$

where, to simplify the notation, $EA := E_s\pi r^2$, $EI := E_s\pi r^4/4$, E_s the Young's modulus of the lattice's constituent material and

$$
\begin{aligned}
&p_1 = 4d_1^2+L_1^2+L_2^2, \qquad p_2 = 4d_2^2+L_1^2+L_3^2, \qquad p_3 = 4d_3^2+L_2^2+L_3^2,\\
&p_4 = p_1^{5/2}p_2^{5/2}\left(L_2^2+L_3^2\right), \qquad p_5 = p_2^{5/2}\left(4d_1^2+L_2^2\right)+L_1^2\left(p_1^{5/2}+p_2^{5/2}\right)+p_1^{5/2}\left(L_3^2+4d_2^2\right),\\
&p_6 = \left(p_2^{5/2}\left(4d_1^2+L_2^2\right)+L_3^2p_1^{5/2}\right), \qquad p_7 = \left(4d_2^2L_1^2p_1^{5/2}+\left(4d_1^2+L_1^2\right)p_2^{5/2}\right)p_3^{5/2}+L_3^2p_1^{5/2}\left(p_2^{5/2}+4d_2^2p_3^{5/2}\right),\\
&p_8 = 16d_2^4\left(4d_2^2+L_1^2+L_3^2\right)p_1^{5/2}p_3^{5/2}+L_2^4p_2^{5/2}\left(p_1^{5/2}+p_3^{5/2}\right), \qquad p_9 = L_2^2p_2^{5/2}\left(L_3^2p_1^{5/2}+\left(4d_1^2+L_1^2\right)p_3^{5/2}\right),\\
&p_{10} = 16d_1^4p_2^{3/2}p_3^{3/2}+L_3^2p_1^{3/2}\left(p_2^{3/2}+p_3^{3/2}\right),\\
&p_{11} = \left(4d_2^2p_1^{5/2}+L_1^2\left(p_1^{5/2}+4d_1^2p_2^{5/2}\right)\right)p_3^{5/2}+L_2^2p_2^{5/2}\left(p_1^{5/2}+4d_1^2p_3^{5/2}\right).
\end{aligned}
\tag{27}
$$

References

[1] Ashby, M., Designing architectured materials, *Scripta Materialia*, vol. 68, pp. 4-7, 2013.

[2] Altenbach, H., Oechsner, A., *Cellular and Porous Materials in Structures and Processes*, Udine, CISM.

[3] Christensen, R. M., Mechanics of cellular and other low-density materials, *International Journal of Solids and Structures*, vol. 37, pp. 93-104, 2000.

[4] Kraynik, A. M., Neilsen, M. K., Reinelt, D. A., Warren, W. E., Foam micromechanics, in: *Foams and Emulsions: Proceedings of the NATO Advanced Study Institute on Foams, Emulsions and Cellular Materials*, Cargese, Corsica, Kluwer, 1998.

[5] Ostoja-Starzewski, M., Lattice models in micromechanics, *Appl. Mech. Rev.*, vol. 55, no 6, pp. 35-60, 2002.

[6] Warren, W. E., Kraynik, A. M., Linear elastic behavior of a low-density Kelvin foam with open cells, *Journal of Applied Mechanics*, vol. 64, pp. 787-794, 1997.

[7] Gibson, L. J., Ashby, M. F., *Cellular Solids. Structure and Properties*, Cambridge University Press, 2001.

[8] Gibson, L. J., Modelling the Mechanical Behavior of Cellular Materials, *Mat. Sci. Eng.*, vol. A110, pp. 1-36, 1989.

[9] Chen, J. Y., Huang, Y., Ortiz, M., Fracture analysis of cellular materials: a strain gradient model, *J. Mech. Phys. Solids*, vol. 46, No. 5, pp. 789-828, 1998.

[10] Kumar, R. S., McDowell, D. L., Generalized continuum modeling of 2-D periodic cellular solids, *Int. J. Solids Struct.*, vol. 41, pp. 7399-7422, 2004.

[11] Gonella, S., Ruzzene, M., Homogenization and equivalent in-plane properties of two-dimensional periodic lattices, *Int. J. Solids Struct.*, vol. 45, pp. 2897-2915, 2008.

DOI: 10.13009/EUCASS2019-167

[12] Brillouin, L., *Wave Propagation in Periodic Structures*, Dover, New York, 1953.

[13] Hutchinson, R.G., Fleck, N.A., The structural performance of the periodic truss, *J. Mech. Phys. Solids*, vol. 54, pp. 756-782, 2006.

[14] Elsayed, M.S.A., Pasini, D., Analysis of the elastostatic specific stiffness of 2d stretching-dominated lattice materials, *Mech. Mater.*, vol. 42, pp. 709-725, 2010.

[15] Vigliotti, A., Pasini, D., Linear multiscale analysis and finite element validation of stretching and bending dominated lattice materials, *Mech. Mater.*, vol. 46, pp. 57-68, 2012.

[16] Born, M., Huang, K., *Dynamical Theory of Crystal Lattices*, Oxford University Press, 1954.

[17] Zhu, H.X., Knott, J.F., Mills, N.J., Analysis of the elastic properties of open-cell foams with tetrakaidecahedral cells, *J. Mech. Phys. Solids*, vol. 45, pp. 319-325, 1997.

[18] Deshpande, V.S., Fleck, N.A., Ashby, M.F., Effective properties of the octet-truss lattice material, *J. Mech. Phys. Solids*, vol. 49, pp. 1747-1769, 2001.

[19] Challapalli, A., Ju, J., Continuum model for effective properties of orthotropic octet-truss lattice material, in: *Proceedings of the ASME 2014*, Montreal, Canada, 2014.

[20] Vigliotti, A., Pasini, D., Stiffness and strength of tridimensional periodic lattices, *Comput. Methods Appl. Mech. Engrg.*, vol. 229-232, pp. 27-43, 2012.

[21] Refai, K., Montemurro, M., Brugger, C., Saintier, N., Determination of the eff??ective elastic properties of titanium lattice structures, *Mechanics of Advanced Materials and Structures*, 2019.

[22] Haghpanah, B., Oftadeh, R., Papadopoulos, J., Vaziri, A., Self-similar hierarchical honeycombs, *Proceedings of the Royal Society of London A*, vol. 469, pp. 5322-5334, 2013.

[23] Vigliotti, A., Pasini, D., Structural optimization of lattice materials, *Proceedings of the ASME 2011*, Washington, USA, 2011.

[24] Venter, G., Review of optimization techniques, in: *Encyclopedia of Aerospace Engineering*, Wiley & Sons, 2010.

[25] Hare, W., Nutini, J., Tesfamariam, S., A survey of non-gradient optimization methods in sructural engineering, *Advances in Engineering Software*, vol. 59, pp. 19-28, 2013.

[26] Zitzler, E., Laumanns, M., Bleuler, S., A tutorial on evolutionary multiobjective optimization, in: *Metaheuristics for multiobjective optimisation*, vol. 535, Springer, Berlin, Heidelberg, 2004.

[27] Konak, A., Coit, D.W., Smith, A.E., Multi-objective optimization using genetic algorithms: a tutorial, *Reliability Engineering and Systems Safety*, vol. 91, pp. 992-1007, 2006.

[28] Vaissier, B., Pernot, J.P., Chougrani, L., Veron, P., Genetic-algorithm based framework for lattice support structure optimization in additive manufacturing, *Computer-Aided Design*, vol. 110, pp. 11-23, 2019.

[29] Burczynski, T., Osyczka, A., *IUTAM Symposium on Evolutionary Methods in Mechanics*, Kluver Academic Publishers, Dordrecht, The Netherlands, 2004.

[30] Abdeljaber, O., Avci, O., Inman, D.J., Optimization of chiral lattice based metastructures for broadband vibration suppression using genetic algorithms, *Journal of Sound and Vibration*, vol. 369, pp. 50-62, 2016.

[31] Anrunaj, E., Hemalatha, G., Ramya, M., Arun Solomon, A., Amudhini Stephen, E., Optimization of regular lattice structure for maximum shear capacity, *International Journal of Engineering and Advanced Technology*, vol. 8, pp. 89-94, 2018.

[32] Dirrenberger, J., Forest, S., Jeulin, D., Effective elastic properties of auxetic microstructures: anisotropy and structural applications, *Int. J. Mech. Mater. Des.*, vol. 9, pp. 21-33, 2013.

[33] Ferreira, A.J.M., *MATLAB Codes for Finite Element Analysis*, Springer Publishing Company, 2009.

DOI: 10.13009/EUCASS2019-167

[34] Nemat-Nasser, S., Hori, M., *Micromechanics: Overall Properties of Heterogenous Materials*, North Holland Publishing, Amsterdam, 1993.

[35] ASTM Standard, *Standard Test Method for Tensile Properties of Plastics*, Designation: D638-14, 2014.

[36] Boyer, R., Welsch, G., Collings, E.W., *Materials Properties Handbook: Titanium Alloys*, eds. ASM International, Materials Park, OH, 1994.